

---

---

# Hadronic Dark Matter Searches at CMS at $\sqrt{s} = 13 \text{ TeV}$

*Searches for invisibly decaying Higgs bosons and semi-visible jets*

---

By

ESHWEN BHAL



School of Physics  
UNIVERSITY OF BRISTOL

A dissertation submitted to the University of Bristol in  
accordance with the requirements for award of the degree  
of DOCTOR OF PHILOSOPHY in the Faculty of Science.

APRIL 2020

Word count: number in words



## ABSTRACT

H ere goes the abstract



## DEDICATION AND ACKNOWLEDGEMENTS

This work is dedicated to my grandfather, Dato' Mahindar Singh Bhal, who was able to begin this journey with me but sadly unable to finish it. There are far too many people and too little space to individually thank everyone who has accompanied me during this PhD, but I'll try my best.

Firstly, to my supervisor, Dr. Henning Flächer. Your advice and guidance over the course of this degree has been instrumental to achieving it, as well as encouraging my growth as a researcher.

Secondly, to all my colleagues at the University of Bristol. Very little would have been achieved without your help. From scientific discussions in the pub to pub discussions in the physics building, they have all been fruitful either directly or by helping me detach from work. Special thanks are in order to Simone and Sam Maddrell-Mander in my cohort, who have put up with my complaining during the stressful times.

To my friends from Monmouth that include my best friends in the world, Mike, James, Sneddon, (Mini) Sam, and Matt Bristow. You've been on this adventure with me since our school days and had my back the entire time. We've been through the highest, lowest, and most hilarious times together. I can definitively say I would not be the person I am today without you.

To my friends from LTA and those based at CERN, especially Dwayne, Vukasin, and Matt Heath. You became my second family while I was in Geneva. I'll miss the skiing, trips into the city, games, and general banter.

To my undergraduate cohort from Exeter. Though our meet ups are rare, I always look forward to our group holidays and hope they continue far into the future.

Lorenza Iacobuzio, you get a special mention. While we weren't especially close until recently, you've been my sage, partner in food, and exceptional friend when I've needed it the most.

Finally, and most importantly, my family deserve my thanks. You have been there for me since the very beginning supporting me through school, undergrad, PhD, and every other endeavour. To my grandparents, uncles, aunties, and cousins, my siblings Joe, Lydia, Sitara, and Arjen, my stepmum Nadia, and my cat Pixie, I am sincerely grateful to have you in my lives. But above all else, to my mum Meeta and dad Kiron, I could not have done any of this without you and as such, you have my deepest and most heartfelt love and gratitude.



## AUTHOR'S DECLARATION

I declare that the work in this dissertation was carried out in accordance with the requirements of the University's *Regulations and Code of Practice for Research Degree Programmes* and that it has not been submitted for any other academic award. Except where indicated by specific reference in the text, the work is the candidate's own work. Work done in collaboration with, or with the assistance of, others, is indicated as such. Any views expressed in the dissertation are those of the author.

SIGNED: ..... DATE: .....



## TABLE OF CONTENTS

	Page
<b>List of Figures</b>	<b>ix</b>
<b>List of Tables</b>	<b>xi</b>
<b>1 Introduction</b>	<b>1</b>
1.1 Evidence for dark matter . . . . .	1
1.1.1 Alternative theories to dark matter . . . . .	3
1.2 Overview of dark matter searches . . . . .	3
1.2.1 Dark matter searches at the LHC . . . . .	5
<b>2 Theory</b>	<b>7</b>
2.1 The standard model of particle physics . . . . .	8
2.2 Limitations of the standard model . . . . .	8
2.3 Theoretical motivations for, and descriptions of, dark matter . . . . .	8
2.4 Important observables in collider physics . . . . .	8
2.4.1 Transverse momentum ( $p_T$ ) . . . . .	8
2.4.2 $H_T$ . . . . .	9
2.4.3 Missing transverse momentum ( $p_T^{\text{miss}}$ ) . . . . .	9
2.5 Measuring the branching ratio of invisibly decaying Higgs bosons . . . . .	9
2.6 Searches for semi-visible jets . . . . .	10
<b>3 The LHC and the CMS experiment</b>	<b>13</b>
3.1 The Large Hadron Collider . . . . .	13
3.1.1 A proton's journey . . . . .	14
3.1.2 Luminosity . . . . .	15
3.1.3 Pileup . . . . .	17
3.1.4 Evolution of the LHC . . . . .	17

---

**TABLE OF CONTENTS**

---

3.2	The CMS experiment . . . . .	17
3.2.1	The CMS detector . . . . .	17
3.2.2	Recording data for analysis . . . . .	17
3.2.3	Jet energy corrections in the Level-1 Trigger . . . . .	17
<b>4</b>	<b>Combined search for the invisible decay of the Higgs boson in hadronic channels</b>	<b>23</b>
4.1	Analysis overview . . . . .	24
4.1.1	Hadronic production modes of the Higgs boson . . . . .	24
4.2	Data and simulation . . . . .	25
4.2.1	Weights and corrections for simulated processes . . . . .	25
4.3	Triggers . . . . .	28
4.4	Categorisation of the non-VBF production modes . . . . .	28
4.5	Background estimation . . . . .	28
4.5.1	Control regions . . . . .	28
4.5.2	Sidebands to the signal region . . . . .	28
4.5.3	Background estimation methods . . . . .	28
<b>5</b>	<b>Search for dark matter through the production of semi-visible jets</b>	<b>29</b>
5.1	Analysis overview . . . . .	30
5.2	Data and simulation . . . . .	30
5.2.1	Generating signal samples in PYTHIA . . . . .	30
5.2.2	Generating signal samples in MADGRAPH . . . . .	30
5.2.3	Triggers . . . . .	30
5.3	Background estimation . . . . .	30
<b>6</b>	<b>Conclusions</b>	<b>31</b>
<b>A</b>	<b>Appendix A</b>	<b>33</b>
	<b>Bibliography</b>	<b>35</b>
	<b>Glossary</b>	<b>41</b>
	<b>Acronyms</b>	<b>43</b>

## LIST OF FIGURES

FIGURE	Page
1.1 A visual representation of the three main types of dark matter detection: direct, indirect, and production . . . . .	4
1.2 The expected masses and interaction cross sections of some dark matter candidates. The centre of mass energy of the LHC is best suited to targeting Weakly Interacting Massive Particles (WIMPs) . . . . .	6
2.1 The typical direction of the missing transverse energy relative to the semi-visible jets as a function of the invisible fraction $r_{\text{inv}}$ . . . . .	11
2.2 Example Feynman diagrams for the two main production modes of semi-visible jets. A $Z'$ boson mediates the $s$ -channel process while a bifundamental $\Phi$ mediates the $t$ -channel process . . . . .	11
2.3 The constituents of a semi-visible jet as a function of its invisible fraction . . . . .	11
3.1 A schematic of the CERN accelerator complex . . . . .	15
3.2 A cutaway diagram of the CMS detector with all of the principal components labelled. This detector configuration was used for the 2017–18 data taking years . . . . .	18
3.3 A transverse slice through the CMS detector with the main subsystems and components visible . . . . .	19
3.4 The integrated luminosity of $pp$ collision data delivered to CMS during 2015 and Run-2 of the LHC . . . . .	19
3.5 The average number of pileup interactions at CMS during 2015 and Run-2 of the LHC . . . . .	20
3.6 Examples of correction curves used to calibrate the jet energies in two $ \eta $ bins . . . . .	21
3.7 The energies of matched pairs of jets in the entire barrel and end cap, before and after jet energy corrections have been applied . . . . .	21

## LIST OF FIGURES

---

4.1 The Feynman diagrams for the four main hadronic production modes of the Higgs boson . . . . .	24
---	----

## LIST OF TABLES

TABLE	Page
3.1 The integrated luminosity delivered by the LHC during Run-2 which were recorded and certified by CMS . . . . .	17



## INTRODUCTION

The universe, in all its vastness, structure, natural laws and chaos, is comprised of only three principal components: visible matter, the ingredients of stars, planets and life, is the only one we interact with on a regular basis; dark energy, a force or manifestation of something even more mysterious, responsible for the accelerating expansion of the universe, is almost entirely unknown; and dark matter, a substance invisible in all sense of the word, that binds galaxies together and influences large scale structure in the cosmos, is the focus of this thesis.

### 1.1 Evidence for dark matter

The earliest evidence for a large, non-luminous component of the galaxy stretches back to the 1920s when Jacobus Kapteyn attempted to explain the motion of stars in the Milky Way [41]. Since then, a wealth of independent astrophysical observations have reinforced the existence of this aggregation not just in our own, but in countless other galaxies and cosmological bodies. The Coma Cluster is a famous example: 90 % of its mass is thought to arise from dark matter, confirmed by its large mass-to-light ratio of  $400 M_{\odot}/L_{\odot}$  [59]. Further evidence is that the rotation curves of most galaxies are roughly flat [47], contrary to the expected Keplerian curve ( $v \propto 1/\sqrt{r}$ ) expected from solely visible matter. On a galactic scale, dark matter is sprinkled in a mostly spherical halo that spans beyond the observable disc. The inclusive dark matter mass increases linearly [28] to compensate for the decline expressed by visible matter [14, 31]. Gravitational lensing is another observational tool subject to be

influenced by dark matter. Images of galaxies and other objects captured by this method appear distorted from a large gravitational field between the source and observer warping its local spacetime [38]. Arcs, ellipses and Einstein rings of smeared galaxies are often seen when dark matter is present.

While there are no widely-accepted estimations, it is believed that 85–95 % of the Milky Way is comprised of dark matter [10, 11, 39]. Though these approximations include non-visible identifiable matter such as dim stars, black holes and neutron stars, the term “dark matter” typically reserved for the non-luminous, *non-baryonic* segment that pervades the cosmos. From the latest results of the Planck mission, the energy density of the observable universe is composed of 26.5 % dark matter [5]. This result follows the Lambda cold dark matter ( $\Lambda$ CDM) model to describe the constituents and evolution of the universe, which is often referred to as the cosmological analog of the standard model of particle physics (SM). From the calculations, postulations, and observations presented above, the following properties of dark matter can be deduced:

- It is electrically neutral since it does not interact with electromagnetic radiation.
- It is cold (non-relativistic). Its velocity within galaxies is similar to the inhabiting stars [13, 36], since the combination of visible and dark matter drives the measured rotation curves. One small caveat is that galactic dark matter would be cold since a velocity above the gravitational escape velocity of the galaxy would eject high speed particles.
- It is stable, at least on the timescale of the current age of the universe. Dark matter production is postulated to have occurred only in the early universe via a thermal freeze out mechanism (see Chpt. 2.3). Hence, the remaining fraction has been present for a considerable time. Since most galaxies are dominated by dark matter and the gravitational influence from only the visible matter is too small to maintain itself, they could not have developed without it. This supports the idea of “bottom-up” structure formation in the universe; smaller galaxies form around gravitational potential wells provided by coalescing dark matter, then merge to form larger structures [58].
- Its interaction with matter and itself is very weak, or even non-existent. The Bullet Cluster – an astronomical object encompassed by two colliding galaxy clusters – is the best example of this inference. From measurements of predominantly x-ray emission and gravitational lensing, it was found that while there is substantial dark matter present, interaction with itself and the visible matter surrounding it was minimal at most [19]. A kinematic explanation for the spherical distribution and low velocity of dark matter

in galaxies can be explained by its collisionless nature. During the formation of a galaxy or stellar system, visible matter frequently collides, dissipating angular momentum and collapsing into a disc.

### 1.1.1 Alternative theories to dark matter

Though little is known about dark matter itself since all evidence stems from its gravitational influence, there are alternative theories that may explain the observations presented above. However, the scientific community can exclude many of these. Mismeasurements of the amount of baryonic matter such as neutrinos, neutrons, and interstellar gas are among the simpler propositions.

The neutrino flux from stars, as well as the cosmic neutrino background [57], are precise and well-tested [REF]. Even considering the upper limits on neutrino masses [45], they cannot make a significant contribution to the dark matter content in the universe. This is even discounting their highly relativistic nature, where myriad experimental evidence suggests dark matter is cold.

One can also use the Cosmic Microwave Background to calculate the average photon and neutrino densities, and Big Bang Nucleosynthesis calculations to determine the baryonic matter density (see Ref. 30 for results with the latest Planck mission data). These can be compared to other measurements, e.g., mass-to-light ratios averaged across the universe, to reveal a discrepancy [25].

Neutrons cannot contribute to dark matter because isolated neutrons are unstable, decaying in a matter of minutes [46]. Transforming into charged protons and electrons, they interact strongly with light and therefore contribute to the luminous matter content.

Modified Newtonian dynamics (MOND) is a hypothesis that aims to explain phenomena typically associated with dark matter instead by modifications to Newton's laws of motion. There exist many theories and interpretations derived from this principle, though any one strand that tries to explain an observation usually fails to satisfy other phenomena or apply to length scales that general relativity may predict well. For example, observations of the Bullet Cluster [19] have discredited many popular MOND models.

## 1.2 Overview of dark matter searches

While observational evidence has so far lain with astrophysics, a theoretical description and discovery of dark matter may fall into the realm of particle physics with the numerous, novel

experimental searches underway. The detection of dark matter can be classified into three distinct methods with unique signatures (with a visual summary in Fig. 1.1):

- **Direct:** dark matter may interact with visible matter on small scales, scattering SM particles [49]. The recoil these SM particles experience could be detected by highly-sensitive, low background experiments such as LUX-ZEPLIN (LZ) [6] that specialises in the search for WIMP dark matter at a large range of masses.
- **Indirect:** if dark matter interacts with itself, it may annihilate to produce showers of high energy photons or pions. Background estimation is difficult since the signatures can be highly model-dependent. The photons may be of a continuum – from hadronisation and radiation of the decay products – or contain features, such as internal radiation from the propagator in the interaction or from loop-level processes [24]. Large ranges of the annihilation cross section and dark matter mass can be probed with telescopes already searching for these characteristic events.
- **Production:** dark matter may have been abundantly produced in the hot, early universe. High energy particle accelerators such as the LHC can reproduce these conditions, with the WIMP miracle (see Chpt. 2.3) reinforcing the idea that dark matter may exist in these accessible mass ranges. Many beyond the standard model (BSM) theories accommodate dark matter candidates with a diverse spectrum of final states that can be investigated by analysing LHC data.

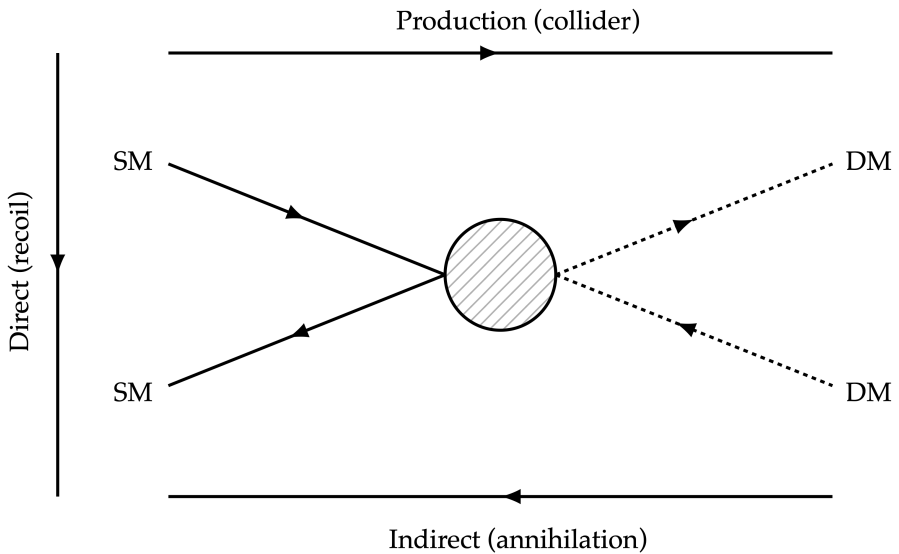


Figure 1.1: A visual representation of the three main types of dark matter detection: direct (dark matter recoiling from standard model particles); indirect (annihilation of dark matter); and production (dark matter created in high energy physics collisions).

### 1.2.1 Dark matter searches at the LHC

Since its detection at the CMS experiment from the production mechanism is the focus of this thesis, it is important to establish the current state of dark matter searches at the Large Hadron Collider (LHC), the world’s most powerful particle accelerator that provides data for CMS. Both machines are described in detail in Chpt. 3, and as such only a summary will be provided here. The LHC principally collides protons at centre of mass energies up to  $\sqrt{s} = 13$  TeV. These exceptionally high energies allow the conditions in the very early universe to be simulated in which heavy, unstable particles were created in abundance. As such, many theories can be investigated that postulate heavy particles that do not exist in the universe today. Some of these, such as supersymmetry (SUSY) [44], sterile neutrinos [27], and Kaluza-Klein states [33] contain dark matter candidates that can be specifically searched for, or indirectly discovered if a theory is experimentally proven. Despite the success of the standard model in explaining the natural world, it does not substantiate the existence of dark matter; hence why BSM theories are popular. Fig. 1.2 illustrates the masses and interaction cross sections of many dark matter candidates. WIMPs (highlighted by the purple rectangle) are the subject of many searches at the LHC since the expected mass ranges and cross sections are accessible there.

Two avenues are usually considered when attempting to discover dark matter: explicit searches for the signatures of dark matter production, and anomalies in precision measurements. The former is quite common, with many theories and models tested at the LHC’s general purpose detectors, ATLAS and CMS. Searches at CMS have been performed for promptly-decaying and “long-lived” supersymmetry in hadronic final states (in which I made contributions) [43, 53]. Searches for specific supersymmetric particles in a variety of decay modes have been conducted by both experiments [16]. In many of these cases, the lightest supersymmetric particle (LSP) is considered to be a dark matter candidate.  $R$ -parity conservation is predicted (or even enforced) in many SUSY models [44], which prevents the decay of LSP and any lighter, standard model particles that have been observed to be stable. While supersymmetry is the most popular BSM theory, due in part to its numerous interpretations and approaches for discovery, many others have also been explored at the LHC. From microscopic black holes [42], to [OTHERS], there are many strategies that have the potential to uproot the standard model. The analyses above are usually characterised by large “missing” transverse momentum (explained further in Chpt. 2.4.3), a quantity that represents the momenta of particles invisible to the detector, which include dark matter. In Chpt. 5, I discuss in detail a search for dark matter that utilises this variable.

Precision measurements of standard model parameters is the other method often consulted

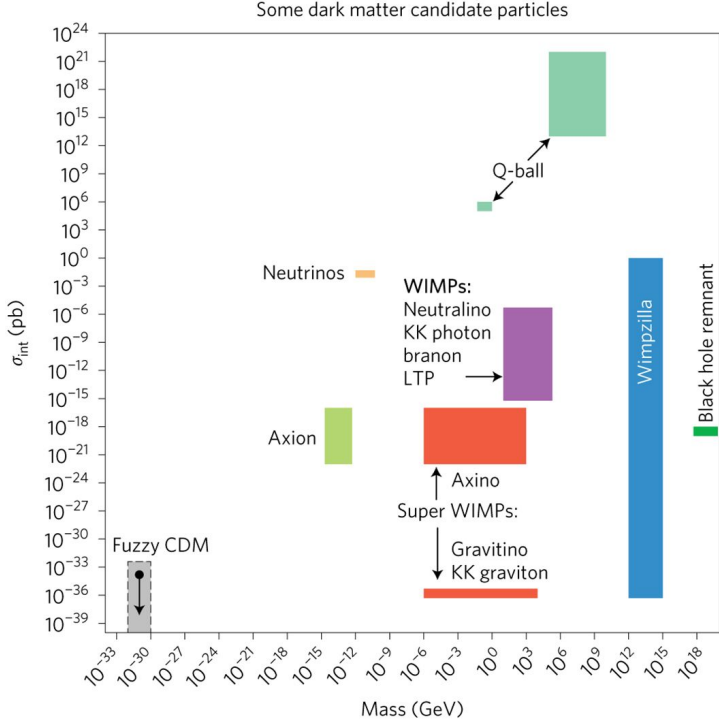


Figure 1.2: The expected masses and interaction cross sections of some dark matter candidates. The centre of mass energy of the LHC is best suited to targeting WIMPs. Figure acquired from Ref. 24.

in the hopes of attributing anomalies to new physics. For example, attempts to explain anomalies in the  $b \rightarrow s$  transition include dark matter candidates [17, 56]. In Chpt. 4, I investigate how the measurement of the Higgs boson to invisible state branching ratio can accommodate dark matter.

There is significant motivation to study dark matter from a wider, as well as a more personal, viewpoint. It is important to understand how the universe operates, and dark matter opens up the potential for new physics that improves our understanding of nature. My personal interests include the blend of particle physics and astrophysics, and the opportunity to discover and add to humanity's collective wisdom. With  $137 \text{ fb}^{-1}$  from CMS during Run-2 at  $\sqrt{s} = 13 \text{ TeV}$ , there is great potential to constrain some of the properties of dark matter. This thesis showcases the motivation for, and results of, searches for invisibly decaying Higgs bosons and semi-visible jets with the full Run-2 dataset collected by the CMS experiment.

## THEORY

This thesis is comprised of experimental searches for dark matter and new physics. The experimental chapters Chpt. 4 and Chpt. 5 delve deeply into the analyses. Before which, the theoretical and phenomenological motivations must be understood to [back up] the need for these searches at the Large Hadron Collider. In this chapter, a brief recap of the standard model will be [presented] along with its shortcomings, i.e., the lack of a dark matter candidate. Theoretical descriptions of dark matter that best fit the relic density and astrophysical observations will then be discussed. Specific interpretations in the form of semi-visible jets and invisibly decaying Higgs bosons are [looked at] that provide the background for the respective analysis chapters.

- Give an overview of the fundamental forces and particles.
- Discuss the Standard Model in detail, emphasising certain aspects as they relate to dark matter and the Higgs field (and boson).
- Briefly recap dark matter, referencing descriptions in introduction. But go into more theoretical descriptions and motivations and how they relate to potentially discovering it at the LHC (WIMP miracle).
- Discuss the theory behind the semi-visible jets analysis (main sources from Refs. 20, 21): strongly interacting dark sector in Hidden Valley scenario with a portal to the visible sector. Mentioning dark quarks  $\chi$ , dark confinement scale  $\Lambda_{\text{dark}}$ , dark hadronisation and decay, running coupling  $\alpha_{\text{dark}}$ , etc.
- Explain some of the phenomenological/experimental event characteristics that overlap

with both analyses, i.e., what a jet is, and maybe energy sums like  $p_T^{\text{miss}}$ ,  $H_T$ ,  $H_T^{\text{miss}}$ , etc.

## 2.1 The standard model of particle physics

## 2.2 Limitations of the standard model

Despite the standard model providing precise predictions of three of the four fundamental forces and the particles that they interact with, there are many experimental observations that it cannot currently explain. Neutrino masses, dark matter, dark energy, and gravity all escape its description.

## 2.3 Theoretical motivations for, and descriptions of, dark matter

The universe may have birthed dark matter via one of many possible mechanisms. The most popular is described as a “thermal freeze-out” process. In the hot, early universe when the thermal background allowed spontaneous pair production of particle dark matter, it was produced in abundance. During this period, they may also have frequently annihilated since the cosmos was still small. Inevitably, the universe expanded and cooled; the temperature became too low to allow significant production [9]. Matter was further separated and the dark matter annihilation rate decreased, leaving a behind the “thermal relic” that is observed today. These remaining particles were attracted via gravity, forming filaments throughout the universe. The potential wells they induced allowed the progenitors of galaxies to form within.

## 2.4 Important observables in collider physics

### 2.4.1 Transverse momentum ( $p_T$ )

In the LHC (or any other collider), the longitudinal momentum of the initial state particles is typically unknown. However, the momentum transverse to the beam is zero before the collision, and therefore must be zero afterward after due to momentum conservation. This is why the transverse momentum of a particle or physics object ( $\vec{p}_T$  for the vector quantity,  $p_T$  for its magnitude) is a useful variable in an analysis.

### 2.4.2 $H_T$

The scalar sum of the transverse momentum of hadronic constituents in an event, i.e., the jets, is symbolised as  $H_T$ . It is often used in analyses focused on hadronic objects, such as natural supersymmetry in which a large jet multiplicity is expected. Formally,

$$(2.1) \quad H_T \equiv \sum_{\text{jets}} p_T$$

Typically, a lower limit on  $p_T$  is used when calculating the  $H_T$ , so jets below this threshold do not factor into the sum. This is to avoid low momentum jets attributed to pileup events (see Chpt. 3.1.3), and those from the primary vertex that can often be mismeasured.

### 2.4.3 Missing transverse momentum ( $p_T^{\text{miss}}$ )

The missing transverse momentum  $p_T^{\text{miss}}$  is defined as the negative vector sum of the  $p_T$  of all identified particles in an event. It is a term often used interchangeably with missing transverse energy (MET,  $E_T^{\text{miss}}$ ). Undetected particles from neutrinos or dark matter, or mismeasured kinematic properties of identified particles, will introduce an imbalance in the vector sum of the  $p_T$ . Hence, the  $p_T^{\text{miss}}$  will be non-zero. Formally,

$$(2.2) \quad p_T^{\text{miss}} \equiv - \sum_i^{N_{\text{particles}}} \vec{p}_{T,i}$$

The hadronic-only counterpart to this variable,  $H_T^{\text{miss}}$ , is the negative vector sum of the jet transverse momenta in an event:

$$(2.3) \quad H_T^{\text{miss}} \equiv - \sum_j^{N_{\text{jets}}} \vec{p}_{T,j}$$

As with  $H_T$ , the  $H_T^{\text{miss}}$  is often calculated with a lower limit on the jet  $p_T$ .

## 2.5 Measuring the branching ratio of invisibly decaying Higgs bosons

The Higgs boson has caught the attention of the high energy physics community and even the public eye like no other particle in recent memory. Its discovery in the  $H \rightarrow \gamma\gamma$  channel

in 2012 by both CMS [18] and ATLAS [3] independently realised one of the [principal] goals of the LHC’s construction. The particle itself is not necessarily exciting. Rather, it confirms the existence of the Higgs *field* that pervades the universe and gives mass to the elementary particles via the exchange of its namesake boson [29, 32, 37]. [Its discovery], one might think, was the end of the discussion of the Higgs boson. However, it was only the beginning.

Many observations of the Higgs, such as its predominant decay mode  $H \rightarrow bb$ , were not seen until recently (CMS [51], ATLAS [1]). Constraints on its other properties have also been placed, such as its resonance width and branching ratios  $\mathcal{B}$  to other final states. Fully understanding the Higgs boson is important to understanding the Higgs field and the wider standard model. Precision measurements in tension with SM predictions can also be a window to new physics. Measuring the  $H \rightarrow \text{inv.}$  branching ratio aims to do just that.

The only SM process in which Higgs boson can decay invisibly is  $H \rightarrow ZZ \rightarrow 4\nu$  with a branching ratio of  $\mathcal{O}(0.1\%)$  [34]. The leading observed experimental upper limits on this measurement are 19 % from CMS [52] and 26 % from ATLAS [2], far above the predicted value. If undiscovered invisible particles, perhaps dark matter, couple to the Higgs field the branching ratio will be enhanced. Experimental evidence shows the coupling strength to proportionally follow the mass of the particle, as verified in ATLAS and CMS’ latest measurements [54]. A considerably large enhancement may allow for this process to be observed at the LHC. At the very least, a more accurate constraint on the branching ratio is able to exclude some models of dark matter, such as those described in Refs. 26, 40.

There is no reason to assume dark matter does *not* interact with the Higgs field, since it bestows mass to all known elementary particles (a small caveat, perhaps, being neutrinos). Higgs “portal” models have been theorised that connect the visible sector of the standard model to a dark sector where particle dark matter resides [7, 8].

## 2.6 Searches for semi-visible jets

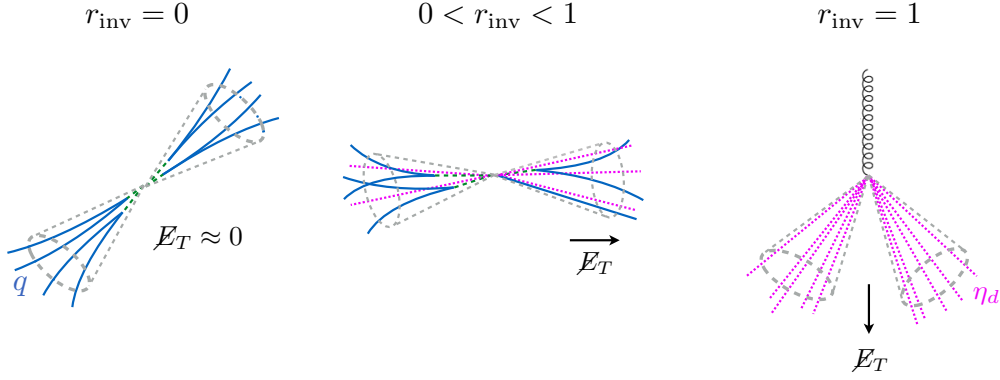


Figure 2.1: The typical direction of the missing transverse energy  $\vec{E}_T$  (or  $p_T^{\text{miss}}$ ) relative to the semi-visible jets as a function of their invisible fraction  $r_{\text{inv}}$  [21].

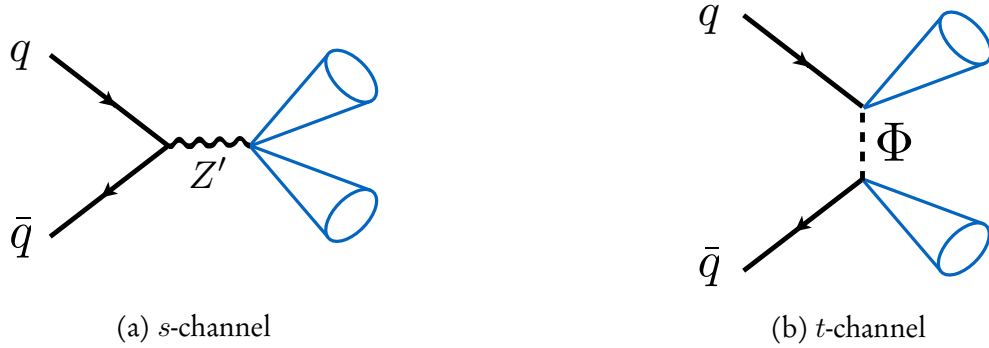


Figure 2.2: Example Feynman diagrams for the two main production modes of semi-visible jets [21]. A  $Z'$  boson mediates the  $s$ -channel process while a bifundamental  $\Phi$  mediates the  $t$ -channel process.

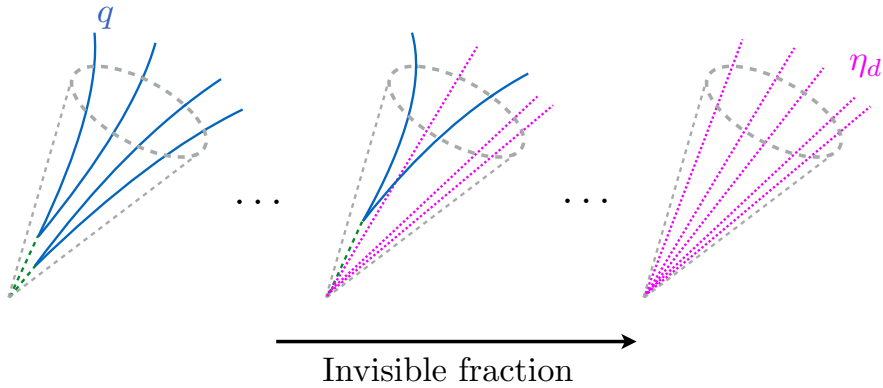


Figure 2.3: The constituents of a semi-visible jet as a function of its invisible fraction  $r_{\text{inv}}$  [21].



## THE LHC AND THE CMS EXPERIMENT

This chapter concerns the experimental setup. The Large Hadron Collider provides the CMS experiment with proton-proton collision data that is then stored, corrected, and then used by physicists for various analyses from standard model precision measurements, searches for new physics, the development of tools and algorithms to aid the previous two, and much more.

- Explain CERN and the LHC in more detail.
- Give an overview of the CMS experiment and detector (including all subsystems, object identification, algorithms for event/object reconstruction like Particle Flow and anti- $k_T$  algorithm, and algorithms for tagging objects like  $b$ -jets). Explain geometry as well ( $\phi$ ,  $\eta$  – with a description (angle between particle/object and beam axis) and equation, also noting the boundaries between barrel, end cap and HF).
- As a subsection in this chapter, discuss the Level-1 Trigger in depth. Emphasise the jet and energy sum triggers as I've worked on them, and Calorimeter Layer-2 for the same reason. Tie into SVJ and Hinv since they're hadronic searches.

### 3.1 The Large Hadron Collider

Deep underground beneath the Franco-Swiss border lies the Large Hadron Collider (LHC), a synchrotron particle accelerator 27 km in circumference. As the largest machine in the world, the LHC stands as a testament to the importance of fundamental science and the

dedication to which it is pursued. Predominantly a proton collider, lead and xenon ions have also been injected for novel and unique studies. Four principle experiments are situated at their own interaction points where the two beams of particles are brought into contact: CMS (Compact Muon Solenoid), a general purpose detector with interests in precision measurements, searches for new physics, and many other avenues; ATLAS (A Toroidal LHC ApparatuS), another general purpose detector with similar aims to CMS; LHCb, designed to study the decay of  $B$  hadrons; and ALICE (A Large Ion Collider Experiment), primarily studying heavy ion collisions and the quark-gluon plasma.

### 3.1.1 A proton’s journey

A proton begins its journey as a hydrogen atom in a little, red bottle. Around  $10^{14}$  protons are supplied to each beam in the LHC, with billions of refills available in this single container. Once the hydrogen atoms leave the source, they are stripped of their electrons, and [sent] to the linear accelerator LINAC2. This is the start of a long voyage through the accelerator complex (visualised in Fig. 3.1).

Given a modest boost to 50 MeV (megaelectron volts), the protons are sequentially fed from LINAC2 into the Proton Synchrotron Booster (PSB) that accelerates them further to 1.4 GeV. Another upsurge is provided once the protons travel to the Proton Synchrotron (PS), this time to 26 GeV. Then the final energy increase received before entering the LHC comes from the Super Proton Synchrotron (SPS), leaving the protons at 450 GeV. Once injected into the LHC, they are finally accelerated to their peak energy of up to 6.5 TeV from a sequence of radio frequency cavities over the course of twenty minutes. The oscillation frequency of these cavities is precisely tuned and timed to give protons the appropriate kicks and accelerate them to the desired energy. Since there is a distribution of proton energies in the beam, those that enter a cavity slightly out of time with a different energy than expected consequently become sorted into “bunches”. The remainder of the LHC ring is used to steer the beam with the aid of over 1,200 liquid helium-cooled superconducting dipole magnets. It is also focused by almost 400 equivalently-cooled quadrupole magnets to increase the rate of proton collisions.

One beam consists of a “train” of up to 2,808 bunches spaced 25 ns apart, each with 115 billion protons. Using bunches provides an advantage to the experiments at each of the interaction points. Discrete collisions take place between bunches in the opposing beams at 40 MHz as opposed to an almost continuous stream of protons. This allows for estimates of pileup interactions that can be filtered out, and would otherwise introduce miscalculations

### 3.1. THE LARGE HADRON COLLIDER

of sums like  $p_T^{\text{miss}}$  and  $H_T$ . Each proton-proton collision is colloquially known as an “event”, with data recorded by each experiment separated into events.

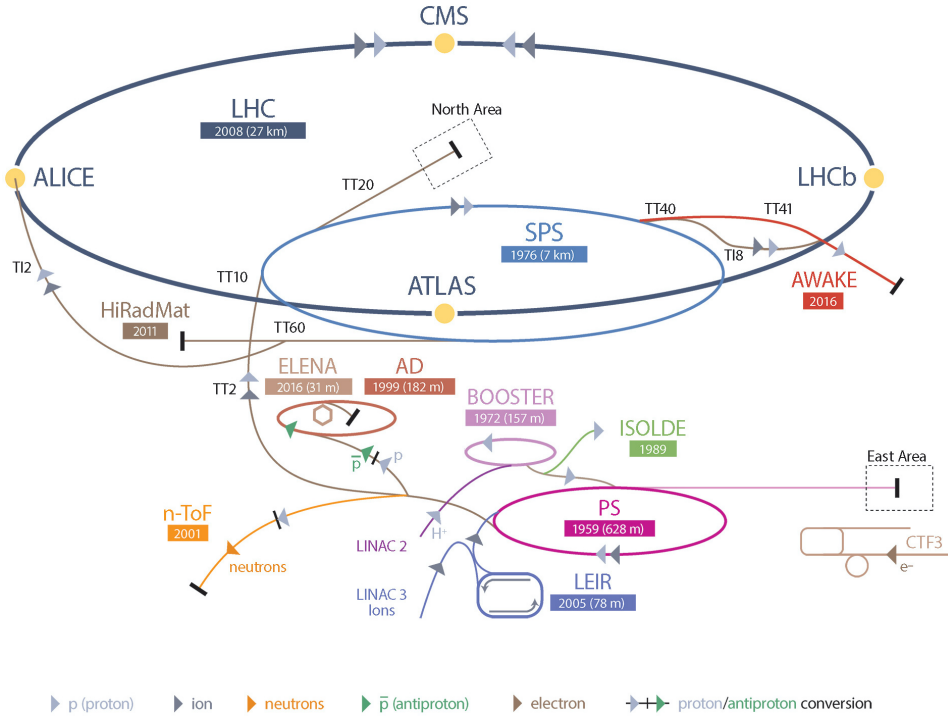


Figure 3.1: A schematic of the CERN accelerator complex. Various particles are shown from their sources to the detectors they are observed at. Figure obtained from Ref. 55.

#### 3.1.2 Luminosity

The *luminosity* of a particle accelerator is, along with centre of mass energy, a quantitative measure of its performance. It is often used to denote the amount of data delivered, or the data collected by the receiving detector. A full derivation of this quantity can be found in Ref. 35, and as such, a summary is given here. The *instantaneous luminosity*  $\mathcal{L}$ , typically quoted in  $\text{cm}^{-2}\text{s}^{-1}$ , is defined as

$$(3.1) \quad \mathcal{L} = \frac{1}{\sigma_p} \frac{dN}{dt}$$

where  $N$  is the number of collisions and  $\sigma_p$  is the production cross section. In the LHC, since many final states are possible,  $\sigma_p$  is not generally known. It can be measured, however. A recent paper from LHCb measured the extrapolated inelastic cross section (which is the important component for LHC collisions) to be  $75.4 \pm 5.4 \text{ mb}$  at  $\sqrt{s} = 13 \text{ TeV}$  [4],

allowing an estimate of the collision rate. For two colliding beams split into bunches with the constituents in each bunch distributed according to a gaussian profile,

$$(3.2) \quad \mathcal{L} = \frac{N_1 N_2 f N_b}{4\pi\sigma_x\sigma_y} \cdot F$$

where  $N_1$  and  $N_2$  are the number of particles in a bunch in beams 1 and 2, respectively,  $N_b$  is the number of bunches in a beam,  $f$  is the revolution frequency (11,245 Hz for protons in the LHC), and  $\sigma_x$  and  $\sigma_y$  are the horizontal and vertical sizes of the beam, respectively.

The geometric reduction factor  $F$  is unity for beams colliding head on. However, in the LHC, the beams collide at an angle known as the “crossing angle” to reduce the effects of pileup. At the start of a fill when the number of protons in the LHC is at its maximum, the crossing angle at each interaction point is approximately 300  $\mu\text{rad}$ . As the runs progress, more protons collide and the luminosity decreases. One of measures taken to recover luminosity and keep the LHC as efficient as possible is to reduce the crossing angle. By the end of the fill, it can be as small as 240  $\mu\text{rad}$ .

The instantaneous luminosity can be increased by the inclusion of more bunches in the beam, decreasing the size of the beam through improved quadrupole magnets, and by reducing the crossing angle. Tuning these parameters led the LHC to reach its design luminosity of  $10^{34} \text{ cm}^{-2} \text{ s}^{-1}$  in 2016. It had more than doubled by the end of Run-2.

Integrating the instantaneous luminosity over a period of time yields the *integrated luminosity*  $\mathcal{L}_{\text{int.}}$ :

$$(3.3) \quad \mathcal{L}_{\text{int.}} = \int \mathcal{L} dt$$

These values are often quoted by experiments in units of “inverse femtobarn” ( $\text{fb}^{-1}$ ) as an indicator of the amount of collision data collected. A “barn” is a unit equal to  $10^{-28} \text{ m}^2$  and colloquially used to express cross sectional area in nuclear and particle physics. As such its reciprocal, the same units as integrated luminosity, gives a good sense of scale that relates cross sections of individual processes to the total amount of data. Tab. 3.1 gives the integrated luminosities over Run-2 delivered by the LHC and collected by CMS. Taking 137.19  $\text{fb}^{-1}$  from this table, and assuming the inelastic  $pp$  cross section above gives an estimate of  $10^{16}$  collisions recorded by CMS over Run-2 (excluding pileup interactions).

### 3.1.3 Pileup

At the high instantaneous luminosity of the LHC, multiple interactions per bunch crossing (known as *pileup*) are frequent.

### 3.1.4 Evolution of the LHC

The LHC began operating in 2010 at a centre of mass energy of  $\sqrt{s} = 7\text{ TeV}$  (teraelectron volts),  $3.5\text{ TeV}$  per beam. A modest increase to  $8\text{ TeV}$  was achieved by the end of Run-1 in 2013. After upgrades were performed, the LHC resumed operation in 2015, further pushing the frontiers of high energy physics with a centre of mass energy of  $\sqrt{s} = 13\text{ TeV}$ . While valuable data was taken, it was not until 2016 when Run-2 of the LHC began. This period ended in 2018 with  $158.64\text{ fb}^{-1}$  of  $pp$  collisions delivered,  $146.45\text{ fb}^{-1}$  of which were recorded by CMS who certified  $137.19\text{ fb}^{-1}$  suitable for analysis [22, 23]. A breakdown by year is presented in Tab. 3.1.

	2016	2017	2018	Full Run-2
Integrated luminosity				
Delivered by LHC ( $\text{fb}^{-1}$ )	40.99	49.79	67.86	158.64
Recorded by CMS ( $\text{fb}^{-1}$ )	37.80	44.98	63.67	146.45
Certified by CMS ( $\text{fb}^{-1}$ )	35.92	41.53	59.74	137.19

Table 3.1: The integrated luminosity delivered by the LHC during Run-2 which were recorded and certified by CMS. Numbers obtained from Refs. 22, 23.

## 3.2 The CMS experiment

### 3.2.1 The CMS detector

### 3.2.2 Recording data for analysis

### 3.2.3 Jet energy corrections in the Level-1 Trigger

Jet energy corrections (JEC) are necessary to compensate for various losses when recording jet properties in the trigger. These losses depend on the transverse momentum  $p_{\text{T}}$  and pseudorapidity  $\eta$ . The calibrations ensure that the performance of the trigger is uniform across the detector. Firstly, some ideal (or reference) jets are needed to compare against given L1 jets. Since Monte Carlo datasets are used for the calibrations, the reference jets we use are the generator-level jets (or GenJets). These are stable, simulated particles clustered with the

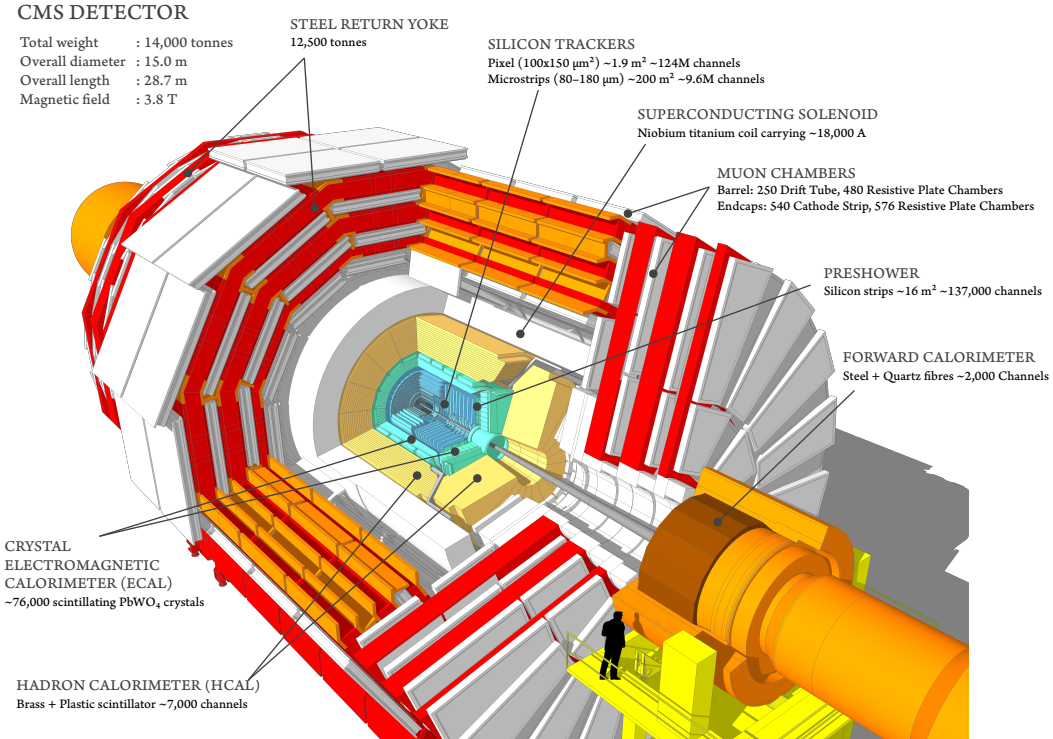


Figure 3.2: A cutaway diagram of the CMS detector with all of the principal components labelled. This detector configuration was used for the 2017–18 data taking years, where the coverage of the pixel detectors in the silicon tracker were upgraded from  $1 \text{ m}^2$  (66 million channels) to  $1.9 \text{ m}^2$  (124 million channels). Image taken from Ref. 48.

anti- $k_T$  algorithm [15] to form the jet. The state of these jets are post-hadronisation, before detector interaction. L1 jets need to be matched against the GenJets. From there, various studies can be performed such measuring the response of the detector  $\langle p_T^{\text{L1}} / p_T^{\text{ref.}} \rangle$ , and its position and energy resolutions.

Once Calorimeter Layer-1 experts have derived scale factors for the physics objects, they are applied in Layer-2 where the calibrations are conducted. For jets, ntuples are created from the specified dataset and the L1 jets are matched to the GenJets using the variable  $\Delta R$ :

$$(3.4) \quad \Delta R = \sqrt{\Delta\eta^2 + \Delta\phi^2}$$

where  $\phi$  is the azimuthal angle of the jet. The algorithm used to match the jets does so by inspecting each L1 jet in descending  $p_T$  and searching for a reference jet with  $\Delta R < 0.25$ . If there is more than one match, the reference jet with the smallest  $\Delta R$  is taken. Then the next L1 jet (and so on) follows the same procedure, with the previous reference jet removed from the matching collection. Calibrations are then derived. The reciprocal of the response vs.  $p_T^{\text{L1}}$

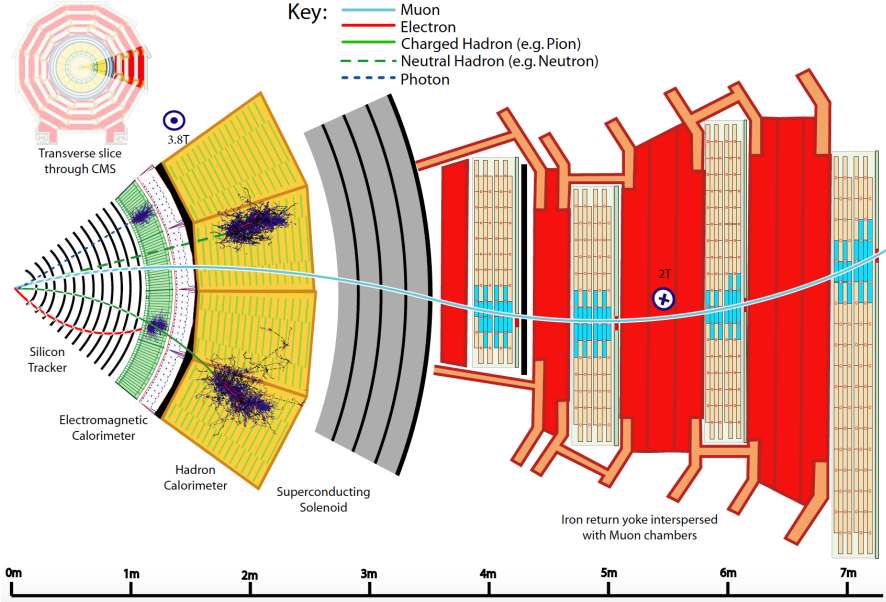


Figure 3.3: A transverse slice through the CMS detector with the main subsystems and components visible (figure obtained from Ref. 50). Several particles produced at the primary vertex and their interactions with the detector are also depicted.

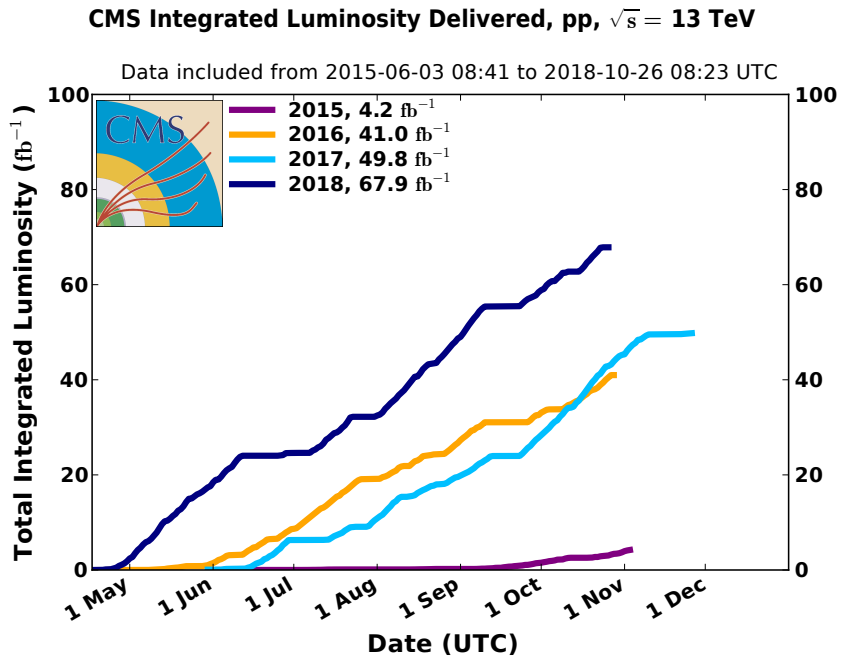


Figure 3.4: The integrated luminosity of  $pp$  collision data collected by CMS during 2015 and Run-2 of the LHC. Figure obtained from Ref. 22.

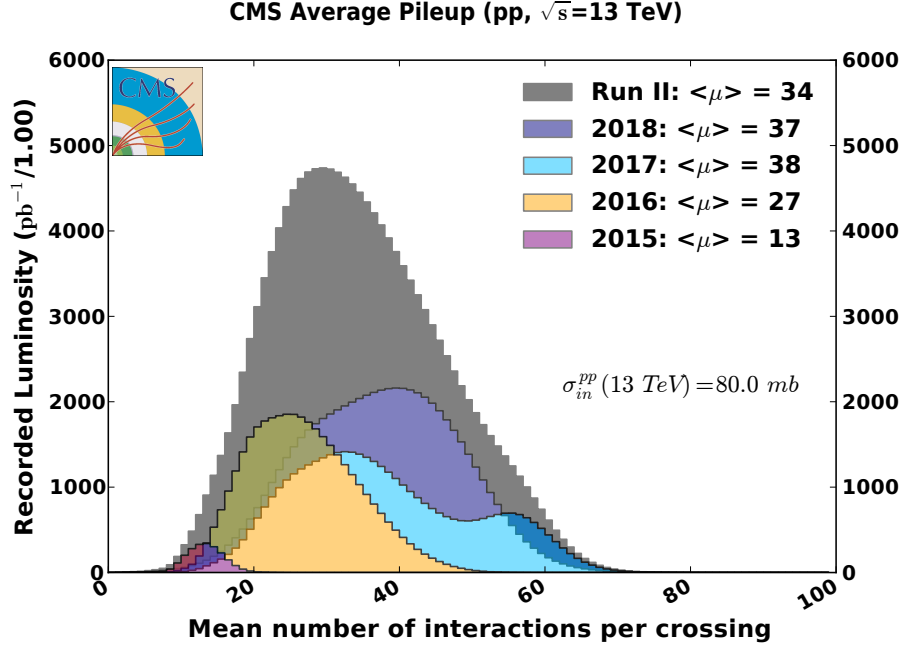


Figure 3.5: The average number of pileup interactions at CMS during 2015 and Run-2 of the LHC. Figure obtained from Ref. 22.

is plotted for each  $|\eta|$  bin and correction curves are fitted to them (see Fig. 3.6). Once tuned such that the fit captures the low- $p_T$  spike and high- $p_T$  plateau, closure tests are conducted as the final step. The ntuples are remade with JECs and then matched with the reference jets to check that the calibrations have been properly applied. Plots such as Fig. 3.7 are then passed to the Trigger Studies Group to check over and continue the chain of trigger corrections and object calibrations.

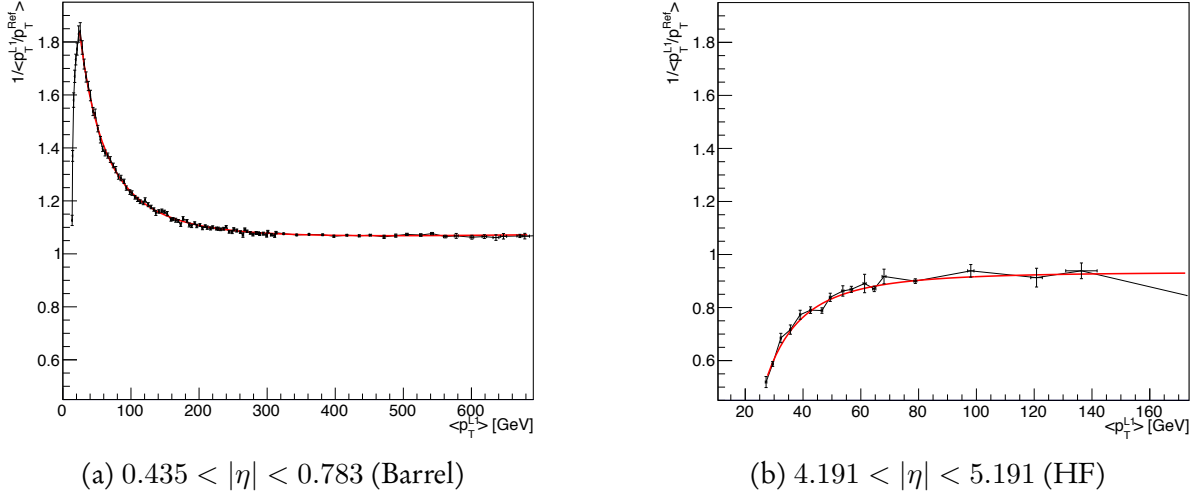


Figure 3.6: Examples of correction curves used to calibrate the jet energies in two  $|\eta|$  bins. The response is plotted against the  $p_T$  of the Level-1 jet and a complex function produces a fit. These plots are from the jet energy corrections performed on 2018 QCD Monte Carlo.

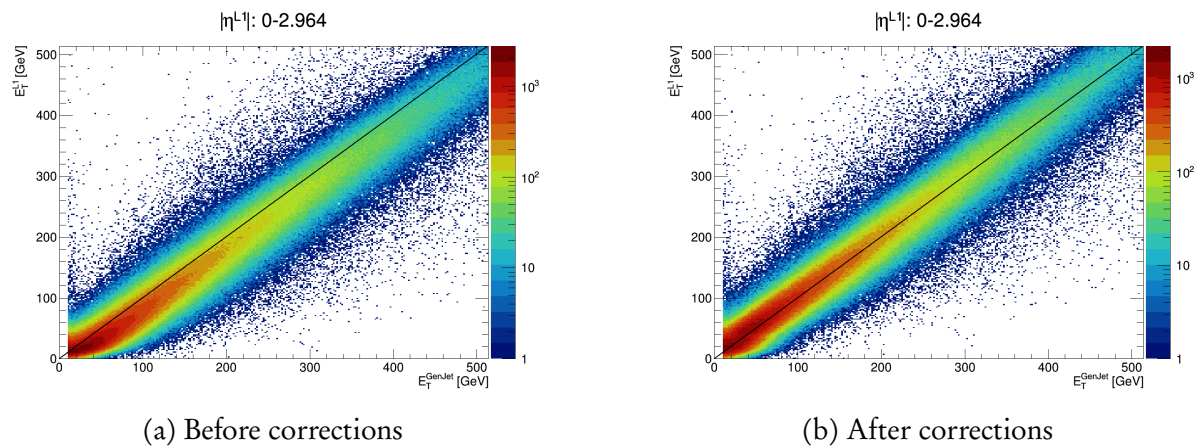


Figure 3.7: The energies of matched pairs of jets in the entire barrel and end cap, before and after jet energy corrections have been applied. After calibrations, the distribution is much more symmetrical. An equivalent plot using jets from LHC data is expected to look similar after applying these calibrations.



## COMBINED SEARCH FOR THE INVISIBLE DECAY OF THE HIGGS BOSON IN HADRONIC CHANNELS

This is the analysis chapter on  $H \rightarrow \text{inv.}$ .

Discuss how the theoretical aspects from the Theory chapter translate into an experimental search.

- Discuss the necessity of including all production modes of Higgs (invisible final state, so characterise events based on initial/additional particles). Also mention how sensitive each production mode is at contributing to the branching ratio limit. Emphasise the non-VBF modes ( $ggF$ ,  $t\bar{t}H$ ,  $VH - W^+H$ ,  $W^-H$ ,  $ZH$ ) in this chapter as that's what I've been working on and another student will be covering VBF.
- Talk about what makes this analysis unique: doing a combination over all production modes from the start instead of separate analyses combined at the end. Means we can share samples, systematics, background methods and workflows, build in orthogonality between the different modes and cover as much phase space as possible (with new final states such as boosted  $Z$  bosons with unresolved subjects). This makes the analysis much more cohesive and consistent.
- Include object definitions, overall analysis strategy, triggers, signal production (with each non-VBF mode in detail), event selection, background estimation and results/limit (including comparisons to previous results).
- Emphasise my contributions: control region construction and studies, background estimation, and other studies I will have conducted by the time I write up.

- Current material: no public plots as of yet. Hope to finish analysis by the time I begin writing up. We are preparing a CMS internal analysis note, documenting all aspects of the analysis. I will add all relevant information there which I can subsequently use when writing this chapter.

## 4.1 Analysis overview

### 4.1.1 Hadronic production modes of the Higgs boson

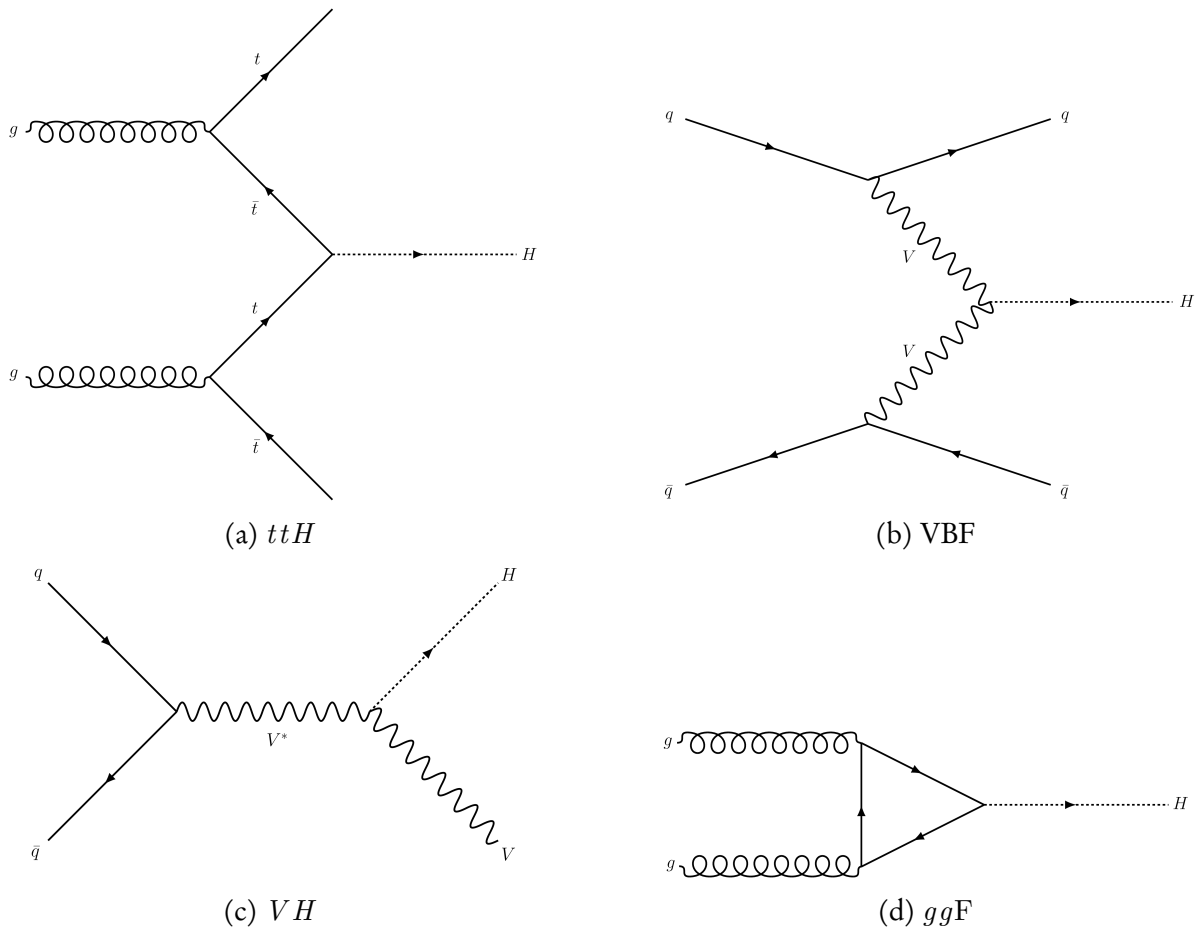


Figure 4.1: The Feynman diagrams for the four main hadronic production modes of the Higgs boson.

## 4.2 Data and simulation

### 4.2.1 Weights and corrections for simulated processes

In order for simulated events, particularly for background processes, to resemble LHC data as closely as possible, many corrections and weights are applied. These are discussed in more detail in the following sections [REF]. A final event weight  $w_{\text{event}}$  is the product of the weights from all of the individual sources  $i$  that provide a weight:

$$(4.1) \quad w_{\text{event}} = \prod_i w_i$$

When representing these events in histograms, the yield in a given bin  $N_{\text{corr.}}$  is the sum of these event weights:

$$(4.2) \quad N_{\text{corr.}} = \sum_j^{N_{\text{MC}}} w_{\text{event } j}$$

where  $N_{\text{MC}}$  is the number of unweighted simulated events in the bin. The statistical uncertainty ascribed to the yield in a bin is given as

$$(4.3) \quad \Delta N_{\text{corr.}} = \pm \frac{N_{\text{corr.}}}{\sqrt{N_{\text{MC}}}}$$

The statistical uncertainty for the number of events in data is simply the Poissonian error

$$(4.4) \quad \Delta N_{\text{data}} = \pm \frac{N_{\text{data}}}{\sqrt{N_{\text{data}}}}$$

The standard prescription for error propagation is to approximate the uncertainty as the square root of the sum of the weights squared [12]:

$$(4.5) \quad \Delta N_{\text{corr.}} = \pm \left( \sum_j^{N_{\text{MC}}} w_{\text{event } j}^2 \right)^{1/2}$$

Our reasoning for using Eq. 4.3 instead of Eq. 4.5 is that the error should be determined purely from the integer number of events we select ( $k$  in a Poisson statistical treatment),

regardless of whether they are weighted or not. This often reduces the uncertainty for MC compared to Eq. 4.5 since many more events are generated to predict a given equivalent luminosity. Further justification is that it is a good approximation in our assumed regime where we expect a large number of events from our MC samples before any cuts are applied (say  $N$ ), and a large enough number of events after the cuts such that we do not encounter the low- $k$  or low- $N$  limits of Poissonian error propagation.

#### 4.2.1.1 Cross section reweighting

Since an arbitrary number of events can be generated for simulation, and a larger number of events gives higher statistical power, events in these datasets need to be reweighted to normalise their contribution to a given region or category. To first order, the weight applied is

$$(4.6) \quad w_\sigma = \frac{\sigma \mathcal{L}_{\text{int.}}}{N \varepsilon}$$

where  $\sigma$  is the cross section of the process at the order it was generated (e.g., on DAS/XSDB for public datasets),  $\mathcal{L}_{\text{int.}}$  is the integrated luminosity of the LHC data it is being compared to,  $N$  is the number of events in the dataset before any skimming (or the sum of the generator weights), and  $\varepsilon$  is the filter efficiency (assumed to be unity for all datasets since no generator-level cuts are applied). If a dataset is generated at leading order, higher order corrections are usually applied on an event-by-event basis that changes the shapes of distributions (see [SEC ON NLO CORRECTIONS]). In some circumstances, “flat” k-factors can be applied to a dataset that only alters the normalisation (i.e., its cross section).

#### 4.2.1.2 Pileup

Pileup interactions at the LHC are frequent (see Chpt. 3.1.3) and must be modelled appropriately in simulation. Simulated samples are generated with a certain distribution of the number of pileup interactions which usually does not match the data recorded by CMS. This is due to changing conditions in the beam over a period of data taking. In order to make them comparable, the simulated events are reweighted; in this context it is known as *pileup reweighting*. ROOT files containing histograms of the number of pileup interactions from short runs in the LHC are available centrally and are used as the reference for which to reweight the simulated events.

In the trees of the simulated samples, the branch `Pileup_nTrueInt` is the mean of the Poisson distribution from which random numbers are drawn. In each simulated event, these

random numbers (all from the same distribution) are used to set the number of in-time pileup interactions as well as the number of the interactions in each neighbouring bunch crossing to simulate the out-of-time pileup. In data, the same branch gives the average number of pileup interactions for a colliding bunch pair in a lumi section. The distribution of Pileup\_nTrueInt in the data is derived from the measured instantaneous luminosity for each colliding bunch pair in each lumi section and the cross section of the total inelastic pp interaction.

The nominal pileup weight, as well as the up and down systematic variations, for each simulated event are derived in nanoAOD-tools.

#### 4.2.1.3 Veto and selection weights

In an analysis, events are often rejected by placing kinematic or object-based requirements. This type of selection strictly removes an event from the analysis if the requirement is not met. While kinematic requirements are either fulfilled or not, a different approach can be used when selecting the number of objects, i.e., when defining control regions. For a set of objects, the selection weight at event level is defined as

$$(4.7) \quad w_{\text{event, sel.}} = \prod_i^{N_{\text{objects}}} \epsilon_i$$

where  $\epsilon_i$  is the efficiency/scale factor applied to object  $i$ . Only reconstructed (“reco” level) objects that have been matched to a generator level object are considered. For leptons ( $e, \mu, \tau$ ) and photons, these scale factors are typically from the reconstruction efficiency, identification efficiency, and  $p_T$  or  $\eta$ -dependent energy corrections. In the case of  $b$ -tagged jets, it is the data-MC scale factor at the given working point of the algorithm used to identify them. These weights are calculated individually for each type of object in an event, and individually for each source since they also introduce systematic variations that cannot be trivially aggregated. A veto weight is defined as

$$(4.8) \quad w_{\text{event, veto}} = \prod_i^{N_{\text{objects}}} 1 - \epsilon_i$$

The uncertainties/systematic variations follow the same prescription. With these quantities defined, an event that meets the object criteria is given the selection weight, otherwise it is given the veto weight. For example, if an event with one muon that meets the criteria for

the  $\mu + \text{jets}$  region will enter that region with its selection weight. That same event can also enter the signal region or one of the sidebands (depending on the event kinematics) with the veto weights. This “migration” of events, where they are able to contribute to more than one region, and the fact that weights are applied instead of event rejection, provides a noticeable decrease to the Monte Carlo statistical uncertainty in a given bin of a given distribution.

One thing must be noted about the migration of events, since we have many different regions of phase space in the analysis. The signal region and the sidebands have orthogonal kinematic requirements, so an event cannot enter the signal region *and* one of the sidebands. The same is true amongst the control regions, i.e., an event cannot enter more than one of them due to the designed orthogonality. An event *is* able to enter the signal region or a sideband with a veto weight, and also one of the control regions with its selection weight. Since events in data are not weighted, they may only enter a single region.

### 4.3 Triggers

### 4.4 Categorisation of the non-VBF production modes

### 4.5 Background estimation

#### 4.5.1 Control regions

#### 4.5.2 Sidebands to the signal region

#### 4.5.3 Background estimation methods

## SEARCH FOR DARK MATTER THROUGH THE PRODUCTION OF SEMI-VISIBLE JETS

This is the analysis chapter on semi-visible jets.

- Discuss how the theoretical aspects from the Theory chapter translate into an experimental search.
- Include object definitions, triggers, overall analysis strategy, signal production, event selection, background estimation and results/limit (including comparisons to similar searches – monojet/dijet exotic searches).
- Emphasise my contributions:  $s$ - and  $t$ -channel signal model production and understanding. Angular variable study for QCD background rejection (if used).
- Current material: no public plots as of yet. Hope to finish  $s$ -channel analysis soon (see previous section for caveats regarding inclusion), no timeline on  $t$ -channel analysis.

## 5.1 Analysis overview

## 5.2 Data and simulation

### 5.2.1 Generating signal samples in PYTHIA

### 5.2.2 Generating signal samples in MADGRAPH

### 5.2.3 Triggers

## 5.3 Background estimation

CHAPTER



## CONCLUSIONS

This is the conclusion.

- Include a summary of thesis and work done over the course of my PhD with emphasis on the most important results/contributions.

- Mention the direction the semi-visible jet and Higgs to invisible analyses can take (sharing ideas/strategies I have, potential improvements with more LHC data and future prospects from potential future experiments).



A P P E N D I X



APPENDIX A

B egins an appendix



## BIBLIOGRAPHY

- [1] M. AABOUD ET AL., *Observation of  $H \rightarrow b\bar{b}$  decays and  $VH$  production with the ATLAS detector*, Phys. Lett., B786 (2018), pp. 59–86.
- [2] ———, *Combination of searches for invisible Higgs boson decays with the ATLAS experiment*, Submitted to: Phys. Rev. Lett., (2019).
- [3] G. AAD ET AL., *Observation of a new particle in the search for the Standard Model Higgs boson with the ATLAS detector at the LHC*, Phys. Lett., B716 (2012), pp. 1–29.
- [4] R. AAIJ ET AL., *Measurement of the inelastic  $pp$  cross-section at a centre-of-mass energy of 13 TeV*, JHEP, 06 (2018), p. 100.
- [5] N. AGHANIM ET AL., *Planck 2018 results. VI. Cosmological parameters*, (2018).
- [6] D. S. AKERIB ET AL., *The LUX-ZEPLIN (LZ) Experiment*, Nucl. Instrum. Meth., A953 (2020), p. 163047.
- [7] G. ARCADI, A. DJOUADI, AND M. RAIDAL, *Dark Matter through the Higgs portal*, Phys. Rept., 842 (2020), pp. 1–180.
- [8] P. ATHRON, C. BALÁZS, A. BENIWAL, S. BLOOR, J. CAMARGO-MOLINA, J. M. CORNELL, B. FARMER, A. FOWLIE, T. E. GONZALO, F. KAHLHOEFER, A. KVELLESTAD, G. D. MARTINEZ, P. SCOTT, A. C. VINCENT, S. WILD, M. WHITE, A. G. WILLIAMS, AND T. G. COLLABORATION:, *Global analyses of higgs portal singlet dark matter models using gambit*, The European Physical Journal C, 79 (2019), p. 38.
- [9] I. BALDES AND K. PETRAKI, *Asymmetric thermal-relic dark matter: Sommerfeld-enhanced freeze-out, annihilation signals and unitarity bounds*, (2017).
- [10] G. BATTAGLIA, A. HELMI, H. MORRISON, P. HARDING, E. W. OLSZEWSKI, M. MATEO, K. C. FREEMAN, J. NORRIS, AND S. A. SHECTMAN, *The radial velocity dispersion profile of the Galactic halo: constraining the density profile of the dark halo of the Milky Way*, Mon. Not. R. Astron. Soc., 364 (2005), pp. 433–442.

## BIBLIOGRAPHY

---

- [11] ——, *Erratum: The radial velocity dispersion profile of the Galactic halo: constraining the density profile of the dark halo of the Milky Way*, Mon. Not. R. Astron. Soc., 370 (2006), pp. 1055–1056.
- [12] P. BEVINGTON AND D. ROBINSON, *Data Reduction and Error Analysis for the Physical Sciences*, McGraw-Hill Higher Education, McGraw-Hill Education, 2003.
- [13] P. BHATTACHARJEE, S. CHAUDHURY, S. KUNDU, AND S. MAJUMDAR, *Sizing-up the WIMPs of Milky Way : Deriving the velocity distribution of Galactic Dark Matter particles from the rotation curve data*, Phys. Rev., D87 (2013), p. 083525.
- [14] A. H. BROEILS, *The mass distribution of the dwarf spiral NGC 1560*, Astronomy & Astrophysics, 256 (1992), pp. 19–32.
- [15] M. CACCIARI, G. P. SALAM, AND G. SOYEZ, *The Anti- $k(t)$  jet clustering algorithm*, JHEP, 04 (2008), p. 063.
- [16] A. CANEPA, *Searches for supersymmetry at the large hadron collider*, Reviews in Physics, 4 (2019), p. 100033.
- [17] D. G. CERDEÑO, A. CHEEK, P. MARTÍN-RAMIRO, AND J. M. MORENO, *B anomalies and dark matter: a complex connection*, The European Physical Journal C, 79 (2019), p. 517.
- [18] S. CHATRCHYAN ET AL., *Observation of a New Boson at a Mass of 125 GeV with the CMS Experiment at the LHC*, Phys. Lett., B716 (2012), pp. 30–61.
- [19] D. CLOWE, A. GONZALEZ, AND M. MARKEVITCH, *Weak-lensing mass reconstruction of the interacting cluster 1e 0657-558: Direct evidence for the existence of dark matter*, The Astrophysical Journal, 604 (2004), p. 596.
- [20] T. COHEN, M. LISANTI, AND H. K. LOU, *Semi-visible Jets: Dark Matter Undercover at the LHC*, Phys. Rev. Lett., 115 (2015), p. 171804.
- [21] T. COHEN, M. LISANTI, H. K. LOU, AND S. MISHRA-SHARMA, *LHC Searches for Dark Sector Showers*, JHEP, 11 (2017), p. 196.
- [22] C. COLLABORATION, *Cms luminosity public results*.  
<https://twiki.cern.ch/twiki/bin/view/CMSPublic/LumiPublicResults>. Accessed 2020-02-22.

- [23] ——, *Luminosity physics object group (lumi pog)*.  
<https://twiki.cern.ch/twiki/bin/viewauth/CMS/TWikiLUM>. Accessed 2020-03-16. Note that access may be restricted.
- [24] J. CONRAD AND O. REIMER, *Indirect dark matter searches in gamma and cosmic rays*, Nature Phys., 13 (2017), pp. 224–231.
- [25] B. COX AND J. FORSHAW, *Universal: A Journey Through the Cosmos*, Penguin Books Limited, 2016.
- [26] A. DJOUADI, A. FALKOWSKI, Y. MAMBRINI, AND J. QUEVILLON, *Direct Detection of Higgs-Portal Dark Matter at the LHC*, Eur. Phys. J., C73 (2013), p. 2455.
- [27] M. DREWES, *The phenomenology of right handed neutrinos*, International Journal of Modern Physics E, 22 (2013), p. 1330019.
- [28] J. EINASTO, *Dark Matter*, ArXiv e-prints, (2009).
- [29] F. ENGLERT AND R. BROUT, *Broken symmetry and the mass of gauge vector mesons*, Phys. Rev. Lett., 13 (1964), pp. 321–323.
- [30] B. D. FIELDS, K. A. OLIVE, T.-H. YEH, AND C. YOUNG, *Big-Bang Nucleosynthesis After Planck*, JCAP, 2003 (2020), p. 010.
- [31] K. C. FREEMAN, *On the Disks of Spiral and S0 Galaxies*, The Astrophysical Journal, 160 (1970), p. 811.
- [32] G. S. GURALNIK, C. R. HAGEN, AND T. W. B. KIBBLE, *Global conservation laws and massless particles*, Phys. Rev. Lett., 13 (1964), pp. 585–587.
- [33] T. HAN, J. D. LYKKEN, AND R.-J. ZHANG, *On Kaluza-Klein states from large extra dimensions*, Phys. Rev., D59 (1999), p. 105006.
- [34] S. HEINEMEYER ET AL., *Handbook of LHC Higgs Cross Sections: 3. Higgs Properties: Report of the LHC Higgs Cross Section Working Group*, CERN Yellow Reports: Monographs, 07 2013.
- [35] W. HERR AND B. MURATORI, *Concept of luminosity*, (2006).
- [36] J. HERZOG-ARBEITMAN, M. LISANTI, P. MADAU, AND L. NECIB, *Empirical Determination of Dark Matter Velocities using Metal-Poor Stars*, Phys. Rev. Lett., 120 (2018), p. 041102.

## BIBLIOGRAPHY

---

- [37] P. W. HIGGS, *Broken symmetries and the masses of gauge bosons*, Phys. Rev. Lett., 13 (1964), pp. 508–509.
- [38] D. HUTERER, *Weak lensing, dark matter and dark energy*, General Relativity and Gravitation, 42 (2010), pp. 2177–2195.
- [39] P. R. KAFLE, S. SHARMA, G. F. LEWIS, AND J. BLAND-HAWTHORN, *On the Shoulders of Giants: Properties of the Stellar Halo and the Milky Way Mass Distribution*, Astrophys. J., 794 (2014), p. 59.
- [40] M. KAKIZAKI, E.-K. PARK, J. HYEON PARK, AND A. SANTA, *Phenomenological constraints on light mixed sneutrino dark matter scenarios*, Physics Letters B, 749 (2015), pp. 44 – 49.
- [41] J. C. KAPTEYN, *First Attempt at a Theory of the Arrangement and Motion of the Sidereal System*, The Astrophysical Journal, 55 (1922), p. 302.
- [42] V. KHACHATRYAN ET AL., *Search for Microscopic Black Hole Signatures at the Large Hadron Collider*, Phys. Lett., B697 (2011), pp. 434–453.
- [43] ——, *A search for new phenomena in pp collisions at  $\sqrt{s} = 13 \text{ TeV}$  in final states with missing transverse momentum and at least one jet using the  $\alpha_T$  variable*, Eur. Phys. J., C77 (2017), p. 294.
- [44] S. P. MARTIN, *A Supersymmetry primer*, Adv. Ser. Direct. High Energy Phys, 18 (1998), pp. 1–98.
- [45] S. MERTENS, *Direct neutrino mass experiments*, Journal of Physics: Conference Series, 718 (2016), p. 022013.
- [46] K. NAKAMURA AND P. D. GROUP, *Review of particle physics*, Journal of Physics G: Nuclear and Particle Physics, 37 (2010), p. 075021.
- [47] M. PERSIC, P. SALUCCI, AND F. STEL, *The universal rotation curve of spiral galaxies - I. The dark matter connection*, Mon. Not. R. Astron. Soc., 281 (1996), pp. 27–47.
- [48] T. SAKUMA, *Cutaway diagrams of CMS detector*, (2019).
- [49] M. SCHUMANN, *Direct Detection of WIMP Dark Matter: Concepts and Status*, J. Phys., G46 (2019), p. 103003.

- [50] A. M. SIRUNYAN ET AL., *Particle-flow reconstruction and global event description with the cms detector*, JINST, 12 (2017), p. P10003.
- [51] ——, *Observation of Higgs boson decay to bottom quarks*, Phys. Rev. Lett., 121 (2018), p. 121801.
- [52] A. M. SIRUNYAN ET AL., *Search for invisible decays of a Higgs boson produced through vector boson fusion in proton-proton collisions at  $\sqrt{s} = 13$  TeV*, (2018).
- [53] A. M. SIRUNYAN ET AL., *Search for natural and split supersymmetry in proton-proton collisions at  $\sqrt{s} = 13$  tev in final states with jets and missing transverse momentum*, Journal of High Energy Physics, 2018 (2018), p. 25.
- [54] A. SOPCZAK, *Precision Measurements in the Higgs Sector at ATLAS and CMS*, PoS, FFK2019 (2020), p. 006. 9 p.  
8 pages, 2 figures, contribution to the International Conference on Precision Physics and Fundamental Physical Constants - FFK2019, 9-14 June, 2019, Tihany, Hungary.
- [55] S. (UKRI), *Cern accelerator complex*.  
<https://stfc.ukri.org/research/particle-physics-and-particle-astrophysics/large-hadron-collider/cern-accelerator-complex/>. Accessed 2020-03-22.
- [56] A. VICENTE, *Anomalies in  $b \rightarrow s$  transitions and dark matter*, Advances in High Energy Physics, 2018 (2018).
- [57] S. WEINBERG, *Cosmology*, Cosmology, OUP Oxford, 2008.
- [58] S. D. M. WHITE AND M. J. REES, *Core condensation in heavy halos: a two-stage theory for galaxy formation and clustering*, Mon. Not. R. Astron. Soc., 183 (1978), p. 341.
- [59] C. YOZIN AND K. BEKKI, *The quenching and survival of ultra-diffuse galaxies in the Coma cluster*, Mon. Not. R. Astron. Soc., 452 (2015), pp. 937–943.



## GLOSSARY

***b*-jet** A jet identified by a given algorithm or classifier as originating from a *b* quark.

**anti- $k_T$  algorithm** .

**jet** A collimated shower of hadronic particles. High momentum quarks and gluons fragment due to colour confinement; the resulting particles deposit energy in the detector very close to each other and is reconstructed as a single physics object called a jet.

**missing transverse energy** The negative vector sum of the transverse momentum of all particles in a collider event. It is sometimes abbreviate to “MET”, and also referred to in literature as “missing transverse momentum” ( $p_T^{\text{miss}}$ ).

**pileup** The term ascribed to additional proton-proton collisions during a bunch crossing. Pileup interactions typically produce a large number of low-momentum particles.

**semi-visible jet** A shower of standard model and dark hadrons from the decay of a leptophobic  $Z'$  or  $\Phi$  mediator that couples the hidden sector to the standard model.



## ACRONYMS

**ALICE** A Large Ion Collider Experiment.

**ATLAS** A Toroidal LHC ApparatuS.

**BSM** beyond the standard model.

**CERN** Organisation Européenne pour la Recherche Nucléaire/European Organisation for Nuclear Research.

**CMS** Compact Muon Solenoid.

**JEC** jet energy corrections.

**LHC** Large Hadron Collider.

**LSP** lightest supersymmetric particle.

**LZ** LUX-ZEPLIN.

**MC** Monte Carlo.

**MeV** megaelectron volt.

**MOND** modified Newtonian dynamics.

**PS** Proton Synchrotron.

**PSB** Proton Synchrotron Booster.

**QCD** Quantum Chromodynamics.

**SM** standard model.

## ACRONYMS

---

**SPS** Super Proton Synchrotron.

**SUSY** supersymmetry.

**TeV** teraelectron volt.

**VBF** vector boson fusion.

**WIMP** Weakly Interacting Massive Particle.